# The very slow solar wind: Properties, origin and variability

Eduardo Sanchez-Diaz, Alexis P. Rouillard, Benoit Lavraud, Kevin Segura, Chihiro Tao, Rui Pinto, N. R. Sheeley, Illya Plotnikov

AGU PUBLICATIONS

JGR

Journal of Geophysical Research: Space Physics

RESEARCH ARTICLE
10.1002/2016JA022433

**Key Points:**
- The solar wind speed extends down to 200 km/s with similar scaling laws as beyond 300 km/s
- Helium abundance, proton mass flux above the photosphere, and photospheric magnetic field have similar solar cycle variability
- The results point out toward a likely influence of collisions in the acceleration of the slow solar wind, regulating the helium abundance

**Correspondence to:**
E. Sanchez-Diaz,
eduardo.sanchez-diaz@irap.omp.eu

**Citation:**
Sanchez-Diaz, E., A. P. Rouillard, B. Lavraud, K. Segura, C. Tao, R. Pinto, N. R. Sheeley Jr, and I. Plotnikov (2016), The very slow solar wind: Properties, origin and variability, *J. Geophys. Res. Space Physics*, *121*, 2830–2841, doi:10.1002/2016JA022433.

Received 29 JAN 2016
Accepted 23 MAR 2016
Accepted article online 30 MAR 2016
Published online 15 APR 2016



# The very slow solar wind: Properties, origin and variability

**Eduardo Sanchez-Diaz[1,2], Alexis P. Rouillard[1,2], Benoit Lavraud[1,2], Kevin Segura[1,2], Chihiro Tao[1,2,3], Rui Pinto[1,2], N. R. Sheeley Jr[4], and Illya Plotnikov[1,2]**

[1]Institut de Recherche en Astrophysique et Planétologie, Paul Sabatier University, Toulouse, France, [2]Centre National de la Recherche Scientifique, UMR 5277, Toulouse, France, [3]National Institute of Information and Communications Technology, Tokyo, Japan, [4]Space Science Division, Naval Research Laboratory, Washington, District of Columbia, USA

**Abstract** Solar wind slower than 300 km/s, hereafter termed very slow solar wind (VSSW), is seldom observed at 1 AU. It was, however, commonly measured inside 0.7 AU by the two Helios spacecraft, particularly during solar maximum. Magnetohydrodynamic (MHD) modeling reveals that the disappearance of VSSW at 1 AU is the result of its interaction with faster solar wind. The acceleration and compression of the VSSW contributes to the observed highly variable structure of the slow solar wind at 1 AU. The VSSW usually contains the heliospheric plasma sheet and current sheet. It has higher density and lower temperature than the regular slow solar wind, extending the known scaling laws below 300 km/s. Its helium abundance increases with solar activity even more significantly than the slow solar wind. Contrary to faster solar winds, the helium ions in the VSSW are slower than the dominant protons. Combining a Potential Field Source Surface (PFSS) model with ballistic back tracing, we study the source region of the VSSW. We show that the proton density flux for the VSSW is much higher than for the faster winds, particularly at solar maximum.

## 1. Introduction

The bimodal nature of the solar wind is very clear when the coronal magnetic field is quasi-dipolar, usually during solar minima. The interplanetary plasma then consists of a dominant quasi-steady fast wind that originates in open-field polar coronal holes and a variable, low-speed wind that originates around the equatorial streamer belt [*McComas et al.*, 2000; *Wilcox and Ness*, 1967]. With increasing heliocentric distance, the fast solar wind interacts with the slower solar wind, thereby reducing the range of velocities of the solar wind [*Collard et al.*, 1982; *Geranios*, 1982; *Burlaga,* 1995]. The most likely places for this interaction are the corotating interaction regions (CIRs), where fast and slow solar wind interact. There, the fast solar wind runs into the slower solar wind ahead producing a compressive interaction [*Pizzo*, 1978, 1980, 1982; *Gosling and Pizzo*, 1999].

The bulk properties of the fast wind (>500 km/s) are less variable, but the latter carries large-scale Alfvén waves more often than the slow solar wind. It originates in cool regions of the corona called coronal holes where the plasma has low freeze-in temperatures ($<1.2\times10^6$ K). The fast wind has a higher helium abundance [*Aellig et al.*, 2001; *Kasper et al.*, 2007, 2012] than the slow solar wind and carries less elements with low first ionization potential (FIP) [*Zurbuchen et al.*, 1999; *von Steiger et al.*, 2000]. The origin of the slow ($300 < V < 500$ km/s) solar wind measured near 1 AU is, by contrast, still highly debated. The high charge-state ratios of $O^{7+}/O^{6+}$ and $C^{5+}/C^{6+}$ typically measured in the slow wind [*Kasper et al.*, 2012] suggest that it originates near hot coronal regions. It has a high abundance of low FIP elements [*Feldman et al.*, 2005], typically detected via spectroscopy in closed coronal loops [*Widing and Feldman,* 2001].

The helium abundance in the slow solar wind is, on average, lower than in the fast solar wind but is highly variable. It can be as low as 1% during solar minimum and as high as 4–6%, more typical of the fast solar wind during solar maximum [*Aellig et al.*, 2001; *Kasper et al.*, 2007, 2012]. In general, the bulk properties and compositional signatures of the slow solar wind are highly variable on all time scales, suggesting that the plasma is released in a highly dynamic manner. The nature and source of this dynamism is still unknown; in particular, it is not clear if the variability is added to the slow solar wind during its acceleration and propagation or if the variability is itself a signature of the formation mechanism of the slow solar wind.

Recent remote-sensing observations of solar wind electrons using heliospheric imaging point to the existence of very slow solar wind structures originating in the vicinity of helmet streamers and propagating to beyond 0.5 AU with slow speeds of around 260 to 300 km/s [see *Rouillard et al.*, 2010a, Tables 1 and 2].

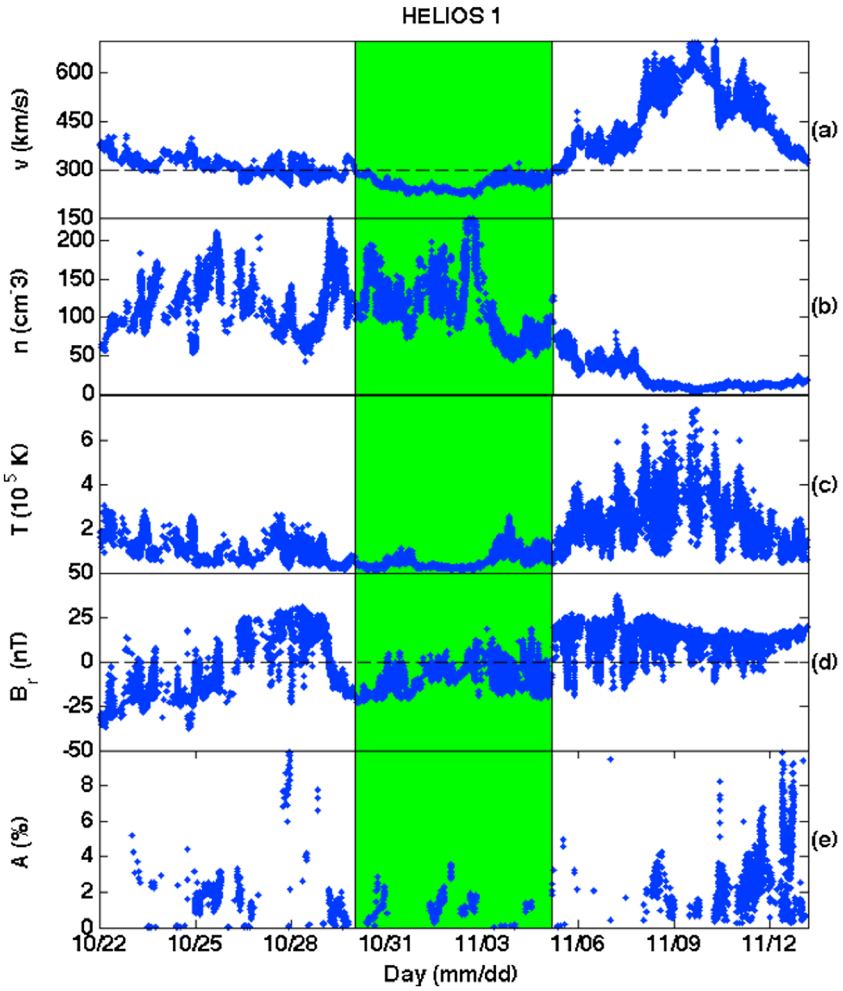


**Figure 1.** Overview plot of Helios 1 data from October 22 to November 12 1977. The (a) proton bulk speed, (b) proton density, (c) proton temperature, (d) radial component of the magnetic field, and (e) helium abundance as a function of time. The green area highlights a particularly broad interval of VSSW with $V < 300$ km/s.

These structures are associated with so-called "streamer blobs" that are thought to be advected passively in the slow solar wind [*Sheeley et al.*, 1997]. If this is true, then in situ measurements taken near 0.3 AU by the Helios spacecraft should have measured such low speeds. Helios 1 and 2 were a pair of spacecraft launched in 1974 and 1976. They were placed in a highly eccentric heliocentric orbit measuring the properties of the solar wind from 0.29 to 1 AU in the ecliptic plane [*Ousley et al.*, 1976]. Both spacecraft had similar instruments providing a unique set of solar wind measurements inside Earth orbit. In this paper, we revisit Helios data and point out the existence of a very slow component of the solar wind (VSSW, $200 < V < 300$ km/s) inside 0.7 AU. A novelty of our analysis with respect to previous studies [e.g., *Marsch et al.*, 1982a, 1982b; *Thieme et al.*, 1989] of the solar wind properties close to the Sun is that it is performed with the full Helios data set, as *Liu et al.* [2005] did for the interplanetary coronal mass ejections (ICMEs). This provides a good statistical significance and allows us to analyze the solar wind evolution over an entire solar cycle.

## 2. The Occurrence of the Very Slow Solar Wind

Figure 1 displays the solar wind parameters measured by Helios 1 during Carrington rotation 1661. The measured solar wind speed decreased to below 220 km/s. The green area corresponds to the period of VSSW ($V < 300$ km/s). In this event Helios 1 encounters a high-density region from 20 October to 3 November. From approximately 27 October to 2 November, this region exhibits changes in the sign of the radial magnetic field component (Figure 1d). Since we do not have concomitant measurements of the suprathermal

**Table 1.** List of Very Slow Solar Wind Events Observed by Helios 1 and 2 Lasting, at Least 24 h With the Starting (Columns 2 and 3) and End (Columns 4 and 5) Date and Time[a]

| Spacecraft | From | | To | | HDR | HPS | HCS |
|---|---|---|---|---|---|---|---|
| 1 | 1975/03/29 | 06:50 | 1975/04/01 | 00:29 | ✗ | ✗ | ✗ |
| 1 | 1975/09/21 | 18:00 | 1975/09/23 | 08:00 | ✓ | ✓ | ✓ |
| 2 | 1976/11/01 | 06:00 | 1976/11/04 | 13:00 | ✓ | ✓ | ✓ |
| 2 | 1976/11/26 | 10:00 | 1976/11/27 | 23:00 | ✗ | ✗ | ✓ |
| 2 | 1977/04/15 | 22:00 | 1977/04/17 | 09:00 | ✓ | ✓ | ✓ |
| 1 | 1977/08/25 | 19:00 | 1977/08/28 | 07:00 | ✓ | ✓ | ✓ |
| 1 | 1977/10/26 | 20:00 | 1977/11/07 | 19:00 | ✓ | ✓ | ✓ |
| 2 | 1977/10/27 | 00:00 | 1977/11/05 | 21:00 | ✓ | ✓ | ✓ |
| 1 | 1977/11/19 | 18:00 | 1977/11/21 | 12:00 | ✓ | ✓ | ✓ |
| 2 | 1977/11/21 | 13:00 | 1977/11/23 | 16:00 | ✓ | ✓ | ✓ |
| 2 | 1978/01/14 | 18:00 | 1978/01/15 | 23:00 | ✓ | ✓ | ✓ |
| 2 | 1978/01/19 | 20:00 | 1978/01/22 | 09:00 | ✓ | ✓ | ✓ |
| 1 | 1978/09/05 | 00:00 | 1978/09/07 | 18:00 | ✗ | ✗ | ✗ |
| 2 | 1978/09/06 | 15:00 | 1978/09/09 | 10:00 | ✗ | ✗ | ✓ |
| 1 | 1978/11/25 | 05:00 | 1978/11/27 | 10:00 | ✓ | ✓ | ✓ |
| 1 | 1979/02/06 | 22:00 | 1978/02/08 | 09:00 | ✓ | ? | no Br data |
| 2 | 1979/04/17 | 13:00 | 1978/04/18 | 13:00 | ✓ | ✓ | ✓ |
| 1 | 1979/05/03 | 10:00 | 1978/05/05 | 01:00 | ✓ | ✗ | ✗ |
| 1 | 1979/05/18 | 05:00 | 1978/05/22 | 16:00 | ✓ | ✓ | ✓ |
| 1 | 1979/06/06 | 06:00 | 1979/06/12 | 16:00 | ✓ | ✓ | ✓ |
| 2 | 1979/10/07 | 15:00 | 1979/10/09 | 16:00 | ✗ | ✗ | no Br data |
| 1 | 1979/10/27 | 01:00 | 1979/10/31 | 08:00 | ✓ | ✓ | ✓ |
| 2 | 1979/10/31 | 10:00 | 1979/11/02 | 03:00 | ✓ | ✓ | no Br data |
| 2 | 1979/11/10 | 17:00 | 1979/11/16 | 16:00 | ✓ | ? | no Br data |
| 2 | 1979/11/23 | 16:00 | 1979/11/24 | 22:00 | ✓ | ? | no Br data |
| 1 | 1979/11/22 | 17:00 | 1979/11/24 | 06:00 | ✓ | ✓ | ✓ |
| 2 | 1980/02/22 | 07:00 | 1980/02/24 | 02:00 | ✓ | ? | no Br data |
| 1 | 1980/05/13 | 09:00 | 1980/05/19 | 01:00 | ✓ | ✓ | ✓ |
| 1 | 1980/05/25 | 15:00 | 1980/05/26 | 15:00 | ✗ | ✗ | ✗ |
| 1 | 1980/05/31 | 12:00 | 1980/06/03 | 12:00 | ✓ | ✓ | ✗ |
| 1 | 1980/06/06 | 06:00 | 1980/06/07 | 10:00 | ✗ | ✗ | ✗ |
| 1 | 1980/06/28 | 16:00 | 1980/06/30 | 22:00 | ✓ | ✓ | ✓ |
| 1 | 1980/09/27 | 10:00 | 1980/09/28 | 12:00 | ✓ | ✓ | ✓ |
| 1 | 1980/12/14 | 06:00 | 1980/12/15 | 22:00 | ✗ | ✗ | ✗ |
| 1 | 1981/06/07 | 01:00 | 1981/06/10 | 12:00 | ✓ | ✓ | ✓ |
| 1 | 1981/12/28 | 01:00 | 1982/01/02 | 17:00 | ✓ | ? | no Br data |
| 1 | 1982/06/30 | 12:00 | 1982/07/03 | 03:00 | ✓ | ? | no Br data |

[a]Additionally, the table reports whether each event is coincident or not with a high-density region (column 6), whether this high-density region is a HPS (column 7), and whether the HCS is lying within the event (column 8).

electrons, we cannot tell if sector boundaries occur at each reversal. However, a crossing of the heliospheric current sheet (HCS) has surely occurred in this period since the radial component of the magnetic field has changed its sign by the end of this interval.

### 2.1. Very Slow Solar Wind Events

We searched the whole Helios data set for periods with at least 24 h of continuous VSSW measurements to identify the presence or not of the HCS in each event. Table 1 contains the VSSW events with at least 24 h of bulk velocity below 300 km $s^{-1}$. The first column identifies the spacecraft, 1 for Helios 1 and 2 for Helios 2. The second and third columns give the start and end dates, respectively, in the format yyyy/mm/dd HH:MM, and the last three columns show the presence (check mark) or not (crosses) of high-density regions (HDR), of the heliospheric plasma sheet (HPS) and/or of the HCS, lying within the VSSW. According to previous definitions [*Crooker et al.*, 2004], we assume the HPS is a high-density region containing a magnetic polarity reversal associated with the passage of the HCS.

The 38 VSSW were identified in the Helios 1 and 2 data sets. VSSW events are on average 3 days long and in 79% of cases have elevated (see HDR list in Table 1) and variable proton densities. Magnetometer data are

available for 30 of the 38 events. The HCS appears in 20 of the 30 VSSW events (67%). During periods of VSSW, the HPS does not stand out as an isolated increase in density in the immediate surrounding of the HCS as typically seen near 1 AU. We could therefore not determine visually if the HPS was really present; however, Table 1 provides a list of likely HPS passages based on the simultaneous detection of the HCS and a HDR. We conclude that the VSSW originates typically from coronal regions situated close to regions forming the HPS and HCS in the direct vicinity of the helmet streamers.

Past studies have argued that complex magnetic field structures are often detected during the passage of the HPS [*Crooker et al.*, 2004]. This is supported by the imaging of small streamer blobs tracked from the top of streamers to 1 AU [*Rouillard et al*., 2010a, 2010b, 2011]. The HPS exhibits at least as variable compositional signatures as the slow solar wind with usually a high charge-state ratio indicative of a hot source regions as well as a higher content of elements with lower FIP than the fast solar wind [*Geiss et al*., 1995]. The alpha-to-proton ratio tends to be low in the HPS [*Borrini et al*., 1981; *Geiss et al*., 1995; *Bavassano et al*., 1997] but is also highly variable and can be at times as high as in the fast solar wind [*Simunac et al*., 2012].

HPS events typically last 6–8 h and at most 16 h at 1 AU [*Crooker et al*., 2004]. Mapped back to the Sun, a 16 h long structure corresponds to a longitudinal angle of 9° for the source region for a synoptic rotation period of 27 days. Accounting for the faster orbital motion of Helios near 0.3 AU which forces some significant corotation of the spacecraft with the Sun, the upper limit of the HPS duration of 16 h event seen near 1 AU maps to 30 h event at Helios (for an assumed synodic rate of 25.38 days). One possible origin for the extended periods of VSSW is a geometrical one; the Helios spacecraft measured VSSW when they traversed large sections of the helmet streamers situated along the ecliptic plane (flat streamers). In this picture, the occurrence of the VSSW is the passage at the probe of a long-lasting crossing of the HPS. We will return to this hypothesis in the discussion section.

### 2.2. Space and Time Distribution of the Very Slow Solar Wind

After analyzing each VSSW period separately, we use the Helios data sets to study the occurrence, the statistical properties and the variability of the VSSW and compare those with the regular slow and fast solar winds. We use the list of ICMEs given by *Liu et al.* [2005] to remove ICMEs. In this list a ICME is defined as a period of combined very high helium abundance (higher than 8%) and low temperature (lower than half the temperature predicted by the scaling law of *Lopez and Freeman* [1986]). In addition, we eliminate all the data with a plasma beta smaller than 0.1 (which means a magnetic pressure of at least 10 times bigger than the plasma pressure). No significant differences were found in the following results between the analysis carried out with and without the removal of ICMEs. Therefore, despite the method used for the ICME removal, the statistical results are representative of the ambient solar wind for our purposes.

As observed in Figure 2 the VSSW is measured at all radial distances inside approximately 0.7 AU and during most of the solar cycle. It is most likely measured near the Sun and during the maximum of the solar cycle (1979–1980). The left hand plot in Figure 2 shows that no wind slower than 250 km/s was ever measured beyond 0.7 AU. The very rare measurements of the VSSW (between 250 and 300 km/s) near 1 AU occur only during solar maximum when high-speed streams are less prominent in the ecliptic plane [*Tokumaru et al*., 2010]. This has been associated with the disappearance of well-defined large-scale coronal holes and their associated extensions in the ecliptic plane and the formation of small and isolated coronal holes at all latitudes [*Wang*, 2010; *de Toma*, 2011].

## 3. Solar Wind Propagation Between 0.3 and 1 AU: Acceleration of the VSSW

Both external heating and interactions with faster winds may give rise to the acceleration of the VSSW, explaining the gradual disappearance of the VSSW with increasing heliocentric distance. To explore whether stream interaction is the mechanism at play to accelerate the VSSW in the interplanetary medium, we propagate solar wind bulk properties in the inner heliosphere out to 1 AU assuming no external heating. We use a 1-D MHD solar wind model described in detail in section 2.1 of *Tao et al.* [2005]. This model solves the MHD equations along the radial direction without any external heating. The initial conditions can be driven by any spacecraft data (here Helios) and all derivatives at the outer boundary (here 1.2 AU) are set to zero. The 1-D MHD equations in a conservative form are given in the cgs Gauss system as

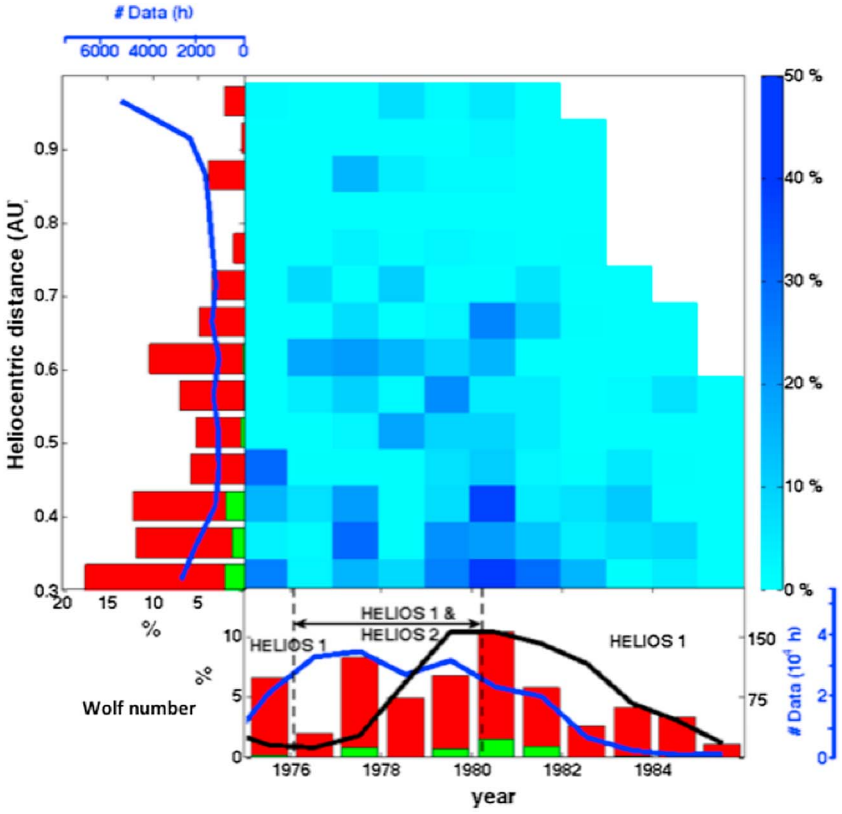


**Figure 2.** (middle) Space-time distribution of the VSSW from all Helios data from 1975 to 1985. For a given year and radial heliospheric distance, the percentage of VSSW ($V < 300$ km/s) is given as the percentage of total wind measured in that time and distance bin, and according to the right-hand side color palette. (left) Time integral of the central plot, showing the percentage of solar wind samples slower than 300 km/s (red) and slower than 250 km/s (green) as a function of heliocentric distance. The blue line represents the amount of data samples, in hours. (bottom) Spatial integral of the central plot, showing the percentage of solar wind samples slower than 300 km/s (red) and slower than 250 km/s (green) as a function of year from 1975 to 1985. The black line represents the yearly averaged Wolf sunspot number, and the blue line shows the amount of data, in hours. Vertical dashed lines show the launch and decommissioning of Helios 2, whose science operations were shorter than Helios 1.

$$\frac{\partial}{\partial t}(\rho S) + \frac{\partial}{\partial x}(\rho v_x S) = 0 \tag{1}$$

$$\frac{\partial}{\partial t}(\rho v_x S) + \frac{\partial}{\partial x}\left[\left(\rho v_x + p + \frac{B^2}{8\pi} - \frac{B_x^2}{4\pi}\right)S\right] = \rho\left[g_x + \left(v_y^2 - \frac{B_y^2}{4\pi\rho}\right)\frac{1}{R}\frac{dR}{dx}\right]S + \left(p + \frac{B^2}{8\pi}\right)\frac{dS}{dx} \tag{2}$$

$$\frac{\partial}{\partial t}(\rho v_y R S) + \frac{\partial}{\partial x}\left[\left(\rho v_x v_y - \frac{B_x B_y}{4\pi}\right)RS\right] = 0 \tag{3}$$

$$\frac{\partial}{\partial x}(B_x S) = 0 \tag{4}$$

$$\frac{\partial}{\partial t}\left(\frac{B_y S}{R}\right) - \frac{\partial}{\partial x}\left[\frac{(B_x v_y - v_x B_y)S}{R}\right] = 0 \tag{5}$$

$$\frac{\partial}{\partial t}\left[\left(\frac{1}{2}\rho v^2 + \frac{p}{\gamma - 1} + \frac{B^2}{8\pi}\right)S\right] + \frac{\partial}{\partial x}\left\{\left[v_x\left(\frac{1}{2}\rho v^2 + \frac{\gamma p}{\gamma - 1}\right) - \frac{1}{4\pi}B_y(B_x v_y - v_x B_y)\right]S\right\} = \rho g_x v_x S \tag{6}$$

where $\rho$, $v$, $B$, and $p$ are the mass density, bulk velocity, magnetic field, and thermal pressure, respectively. The gravity is $g_x = -GM/x^2$, where $G$ is the gravitational constant and $M$ the mass of the Sun. The unit surface $S$ is defined as the square of the heliocentric distance, $x$, and $R(x) \approx x$ is the distance to the solar rotation axis.

Figure 3 shows the radial speed measured by Helios 1 (blue) and the output of the MHD model at several heliocentric distances up to 1 AU (red) for the time period between 1 and 10 May 1979. This example shows

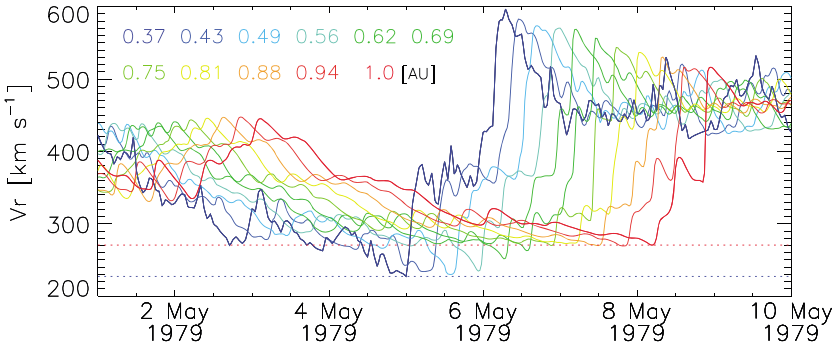


**Figure 3.** The radial velocity of the solar wind measured by Helios 1 between 1 and 10 May 1979 is shown by the dark blue solid line. The radial velocity outputs of the 1-D MHD propagation model are presented for different heliocentric distances with the rest of the colored solid lines. The colored numbers on the top left side stand for the average heliocentric distance of Helios 1 (dark blue) and each output during this time period. The dashed lines show the minimum velocity of Helios 1 measurement (dark blue) and that of model output at 1 AU (red).

that the 1-D MHD equations, without any source of external heating, predict the acceleration and disappearance of all VSSW below 270 km/s (horizontal dashed red line) at 1 AU. The fastest velocities also disappear by 1 AU (see largest speeds between 6 and 9 May), pointing to a deceleration process. The interaction between the slow and fast solar wind thus produces an overall reduction in velocity differences during propagation.

In order to explore the nature of this interaction, we computed the values of the different terms in equation (2) around the VSSW events. The gradient of dynamic pressure $(\frac{\partial}{\partial x}(\rho v_x^2 S))$ is at least 1 order of magnitude higher than all the other terms added together, for the particular solar wind characteristics (from Helios data). This shows that the acceleration of the VSSW and the associated disappearance of the very slow speeds is indeed associated with high dynamic pressure gradients owing to the interaction with faster winds that are known to happen in stream interaction regions [*Burlaga*, 1995].

## 4. The Properties of the Very Slow Solar Wind

The distributions of some measured bulk plasma parameters and derived quantities are presented in Figure 4 as a function of speed, ranging from 200 to 700 km/s.

Note that the $R^{-2}$ variation of the density assumed in Figure 4b may be affected by compression and rarefactions in stream interactions. In order to minimize the error of scaling the in situ measurements to a common distance, we only include the measurements inside 0.7 AU in Figures 4a–4d

The proton temperature and density of the VSSW appear as a continuation of the regular slow solar wind at lower speeds: the slower velocities correspond to even lower temperatures, higher densities, and higher proton fluxes (Figures 4a–4c). There is a slight increase in the helium abundance of the VSSW (Figure 4d) relative to the solar wind with speeds $300 < V < 350$ km/s.

To determine the properties of the coronal source regions of the solar wind, the point on the source surface—a sphere centered on the Sun with a radius of 2.5 solar radii ($R_S$)—that emitted each plasma element measured by Helios is found by a simple ballistic back tracing method using the speed of the solar wind measured in situ, the heliographic coordinates of Helios, and an assumed solar rotation period of 26.38 days. Below 2.5 $R_S$ a PFSS model [*Schatten et al.*, 1969] is used to trace this point back to the photosphere. Carrington maps from the Mount Wilson Observatory (MWO) are used as input for the PFSS model. Finally, the proton flux is traced from Helios back to the source surface and to the photosphere assuming constant proton flux along a magnetic flux tube:

$$\frac{N_p V_p(\text{Helios})}{B_r(\text{Helios})} = \frac{N_p V_p(\text{source} - \text{surface})}{B_r(\text{source} - \text{surface})} = \frac{N_p V_p(\text{photosphere})}{B_r(\text{photosphere})} \quad (7)$$

where $N_p$ and $V_p$ are the proton density and the proton bulk velocity in the direction of the magnetic field and $B_r$ is the radial magnetic field.

Figures 4e–4h present the properties of the coronal source regions of the solar wind as a function of solar wind speed. The expansion factor, FS, (Figure 4e) is defined as

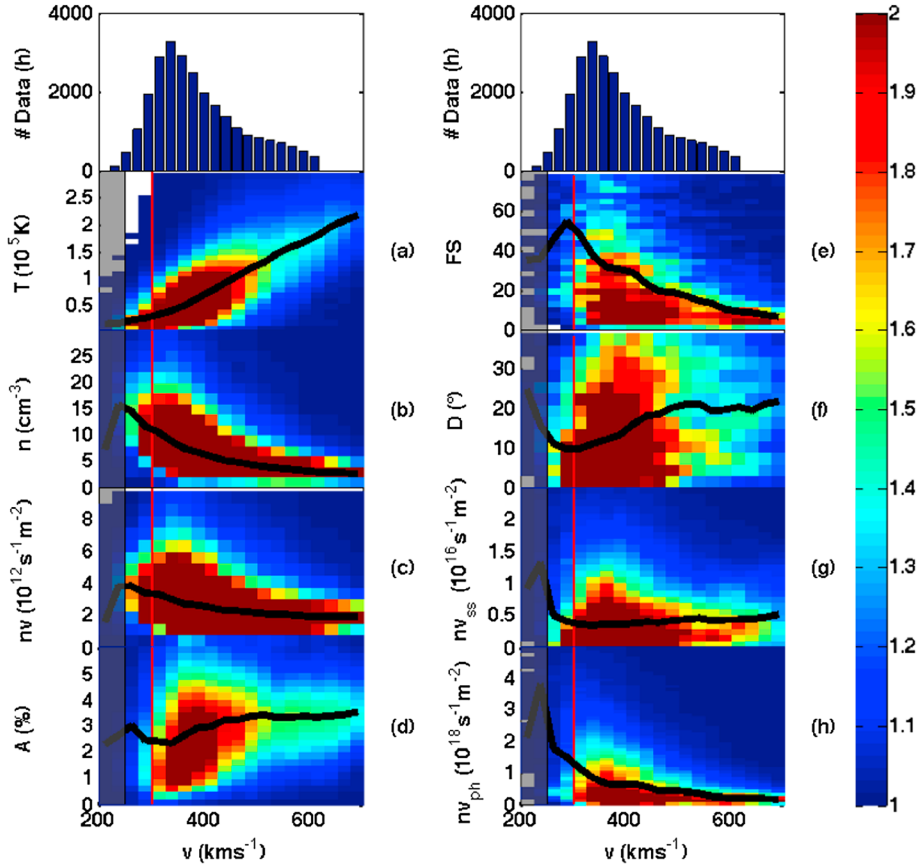


**Figure 4.** For each panel, using the entire Helios 1 and 2 data sets, excluding ICMEs, we display the percentage of samples for a given pair of values (*V*, *Y*) where *V* is the solar wind speed and *Y* the property on the *Y* axis. The black line shows the median of that quantity for each velocity interval. (a–d) The quantities directly measured in situ and (e–h) the properties at the Sun resulting from tracing the in situ measurements back to the Sun. The corresponding quantities are the following: (Figures 4a–4d, measured in situ) proton temperature, proton density, proton flux, He abundance, (Figures 4e–4h, back traced) field line expansion factor, distance to the photospheric neutral line and proton flux at the source surface, and above the photosphere. The red vertical line is at 300 km/s to separate the slow solar wind from the VSSW. On top of each column a histogram shows the distribution of all Helios samples (in units of time). The properties below 250 km/s lack sufficient statistics (less than 200 h of measurement) and are thus shaded in grey to highlight the necessary caution with this interval. Bins have a size of 25 km/s and cover a speed range from 200 km/s to 700 km/s. In Figures 4a–4d, the proton density and proton flux are scaled to 1 AU with a $R^{-2}$ dependence and the temperature with $R^{-0.7}$ [*Ebert et al.*, 2009]. Only data inside 0.7 AU are included.

$$\mathrm{FS} = \left(\frac{R_0}{R_s}\right)^2 \frac{B_r(R_0)}{B_r(R_s)} \tag{8}$$

where $R_0$ is the solar radius, $R_S$ the radius of the source surface, and $B_r$ is the radial component of the magnetic field. The expansion factor measures the super radial expansion of the magnetic flux tubes from the photosphere to the source surface. The distance to the neutral line, *D*, (Figure 4f) is the minimum distance between the source of the solar wind and the photospheric neutral line. The values for $B_r(R_0)$ and $B_r(R_s)$ are taken from the Carrington maps from MWO.

Figure 4e retrieves the well-known result that the solar wind speed is generally anticorrelated with the expansion factor. The expansion factor of the VSSW is high, comparable to the expansion factor of the slow solar wind and higher than the expansion factor of the fast solar wind. The source region of the VSSW is located near the coronal neutral line (Figure 4f).

Even though the slow solar wind originates in rapidly expanding flux tubes, the slow and VSSW carry a proton mass flux at the source surface that is slightly higher than the fast wind (Figure 4c). It is likely, therefore, that they also have very high proton mass flux just above the photosphere or transition region [*Wang*, 2010]. As noted in previous studies, the proton flux at the source surface is independent of the solar wind speed (Figure 4g),

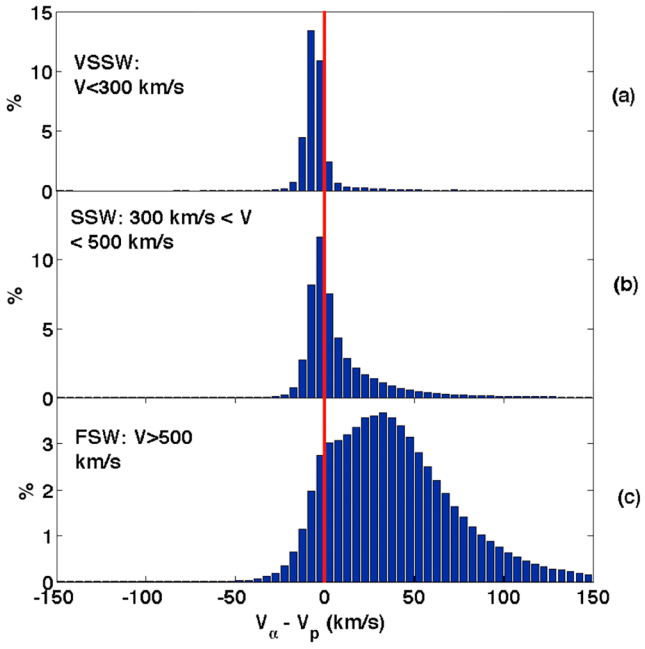


**Figure 5.** (a) Percentage of VSSW, (b) slow solar wind, and (c) fast solar wind with the alpha-proton speed difference shown in the *x* axis. The red line separates $V_\alpha < V_p$ (left) from $V_\alpha > V_p$ (right).

except for a small increase in the VSSW. However, the proton flux computed just above the photosphere (by tracing flux tubes from the source surface sunwards) in the VSSW is an order of magnitude higher than in the fast solar wind.

Many studies argue that the fast solar wind is heated by wave-particle interactions [e.g., *Hollweg and Isenberg*, 2002]. In this picture, assuming typical power law spectra for the waves in the corona, helium ions, which for equal energy have larger gyroradii than protons, resonate with the large amplitude waves and extract first energy from the cascading spectrum of waves and leaving less wave energy to the protons. This could provide a mechanism by which helium could move faster and be hotter than hydrogen in the fast solar wind [e.g., *Maneva et al.*, 2015]. The histograms of the relative alpha-to-proton speed for the VSSW (Figure 5a), regular slow (Figure 5b), and fast (Figure 5c) winds show that the fast wind presents a wide range of relative velocities, with helium being preferentially faster. By contrast, in the VSSW, helium ions are preferentially slower and there is a narrower distribution of relative velocities. Thus, relative alpha-to-proton speeds tend to be small and negative in the VSSW.

## 5. Solar Cycle Variability

The expansion of the flux tubes and the strength of the magnetic field at their base have been proposed as critical parameters regulating the properties of the solar wind ultimately measured in situ [*Wang*, 1995; *Wang et al.*, 2009]. The magnetic field topology continuously evolves during the solar cycle from a quasi-dipole at solar minima to complex topologies at solar maxima. Figure 6 shows the median of the helium abundance (a), the proton flux right above the photosphere (b), the photospheric magnetic field strength at the photosphere (c), and the expansion factor (d) as a function of time during the solar cycle for different solar wind speeds.

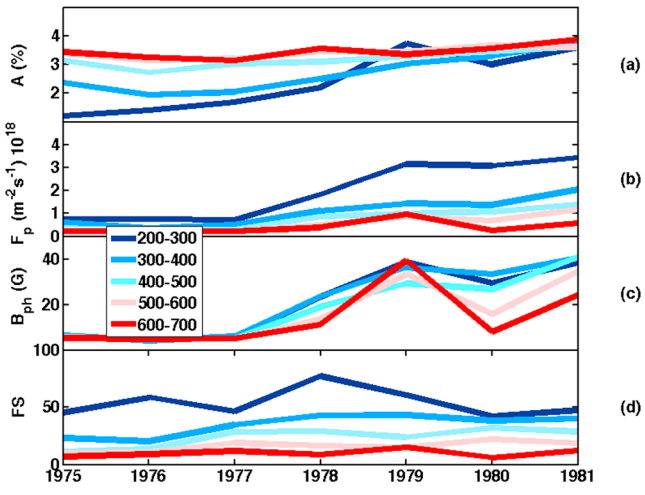


**Figure 6.** Yearly evolution of (a) the helium abundance, (b) the proton flux above the photosphere, (c) the photospheric magnetic field strength, and (d) the expansion factor corresponding to different velocity intervals according to the color coding given on Figure 6c. The slow solar wind (<500 km/s) is assigned blue colors, and the fast solar wind (>500 km/s) is represented by red colors.

The VSSW has the lowest helium abundance at solar minimum but

has high abundances at solar maximum, comparable to faster solar winds, with a fairly continuous transition between these two phases of the solar cycle. The VSSW is more frequent at solar maximum when the solar wind is generally more helium abundant (Figures 2 and 6a). For this reason values averaged over the whole solar cycle and shown in Figure 4 are more representative of solar maximum than solar minimum.

The proton mass flux above the photosphere in the VSSW is always higher than in the faster winds. It also increases dramatically at solar maximum, leading to a very high median proton flux for the VSSW. The helium abundance, the photospheric magnetic field, and the proton flux above the photosphere are all well correlated with solar activity. In addition, these three quantities show similar trends over the years for the slow and the VSSW.

A striking feature seen in Figure 6 is that the helium abundance in all types of winds, including the VSSW, reach a common maximum value at solar maximum of just under 4% corresponding to the abundance measured in the fast solar during cycle 21. *Kasper et al.* [2012], who measured the same feature for solar cycle 23, argued that a common heating mechanism is regulating the helium abundance in the fast and slow solar wind at solar maximum.

## 6. Discussion

We point out the frequent occurrence of solar wind plasma slower than 300 km/s near Helios perihelion. It can be at times as slow as 200 km/s inside 0.7 AU, a speed never measured at 1 AU. The propagation of the solar wind modeled using MHD from Helios out to 1 AU for one of the periods shows that, when the VSSW is associated with high dynamic pressure gradients, these pressure gradients accelerate the VSSW up to regular slow solar wind speeds. The disappearance of the VSSW reported here inside 0.7 AU is thus most likely associated with the interaction between the VSSW and faster solar winds during their propagation. The VSSW becomes part of the "regular" slow solar wind at 1 AU. However, it typically has lower temperatures and higher densities than the regular slow solar wind. We thus suggest that the acceleration and compression of the VSSW must contribute to the observed highly variable structure of the slow solar wind measured near 1 AU.

The reported in situ measurements suggest that the properties of VSSW are a continuation of the slow wind toward lower speeds: higher densities, higher proton fluxes, and lower temperatures, thereby extending well-known scaling laws [*Lopez and Freeman,* 1986; *Hundhausen et al*., 1970] down to speeds as low as 200 km/s.

The back tracing of in situ measurements to the photosphere shows that in the slowest wind, the proton flux above the photosphere is anticorrelated with the proton bulk speed. The dependence of the proton flux at the photosphere on solar wind speed is remarkable (Figures 4h and 6b). Due to the limitation of the back tracing method and the resolution of the PFSS computation employed we could not tell whether the VSSW originates closer to the photospheric neutral line (Figure 4f) than the slow solar wind. However, we have found that periods of VSSW are often associated with the passage of the HCS (Table 1). These combined observations suggest that the VSSW originates very near the tip of the helmet streamer.

The helium abundance is much lower in the VSSW than in the slow wind but at solar minimum only (Figure 6 a), this is qualitatively consistent with a continuation of the slow solar wind during solar minimum [*Aellig et al*., 2001; *Kasper et al*., 2007, 2012]. These solar minimum measurements support the idea that the VSSW events are long-lasting crossings of the HPS because measurements of the HPS near 1 AU are typically marked by sharp decreases in helium abundance [e.g., *Simunac et al*., 2012]. At 1 AU, the clearly identified HPS passages are of short duration and are marked by discontinuous increases in proton density. These short HPS events are usually associated with spacecraft crossings of the neutral line or equivalently north-south ("vertically") orientated streamers [e.g., *Simunac et al*., 2012]. VSSW periods measured near Helios were here traced back to E-W extensions of the helmet streamers situated in the ecliptic plane.

Our analysis based on Helios data confirms the results of *Kasper et al.* [2012] using data from near-Earth orbiting spacecraft, showing that the helium abundance of the slow solar wind changes with solar activity. We here show that helium abundance can become at solar maximum as high or even at times higher in the VSSW than in the fast wind. If the VSSW is indeed associated with the HPS, then the helium abundance in the HPS must also vary with the solar cycle. To our knowledge, no study has yet investigated the cause of such a possible variation and we seek to investigate this idea in a future study.

The well-known observation that helium flow speed at 1 AU is equal to or greater than the proton speed for fast solar wind is also seen in Helios measurements closer to the Sun for wind speeds greater than 300 km/s

(Figure 5c). Recent measurements indicate that alpha particles measured near Earth can be nearly seven times hotter than protons [*Kasper et al*., 2008]. The origin of such strong heating of the alpha particles in the fast wind is still an open question. Helium faster than protons cannot be interpreted by simply invoking the effect of gravity, outwardly directed charge separation electric fields, pressure gradients, nor Coulomb frictions. To interpret the faster helium measured in the fast solar wind, collisionless processes such as wave-particle interactions have been proposed to preferentially heat helium and boost its speed. In the Alfvén-wave driven solar wind model [*Hollweg and Isenberg,* 2002], the different alpha and proton terminal speeds are explained by different responses of alpha particles and protons to wave-particle interactions associated with their different masses and resonance conditions [*Barnes*, 1968; *Dusenbery and Hollweg,* 1981].

The high-proton densities measured in situ in the VSSW in spite of the large expansion factors between the photosphere and the source surface point to significant proton mass fluxes traced back to the photosphere. The variation of the mass flux in the slowest winds during the solar cycle is well correlated with the variation of the helium abundance in the VSSW. This correlation holds less true for faster winds with overall decreasing average mass flux as reported here. Unlike the photospheric mass flux (Figure 6b), the expansion factor does not exhibit significant variations during the solar cycle (Figure 6d). Therefore, the expansion factor is likely not regulating the variability of the mass flux. By contrast, the proton mass flux and the photospheric magnetic field follow similar trends during the solar cycle (Figures 6b and 6c). If the footpoint field strength controls the heating rate at the coronal base, then we should also observe an enhanced mass flux at that base [*Wang et al*., 2009]. The cycle variation of the mass flux derived here may result from the changing topology of the corona. At solar maximum, the slow solar wind could originate primarily from isolated coronal holes in contrast to solar minimum when the slow wind emerges from the boundary of the polar coronal holes [*Wang et al*., 2009]. Isolated coronal holes situated near active region belts have stronger footpoint field strengths than polar coronal hole boundaries.

Solar wind acceleration models that parameterize the heating rate to the geometry of magnetic flux tubes relate the fast solar wind to efficient heating mechanisms acting from the transition region to several solar radii along weakly expanding magnetic flux tubes. In contrast, the heating along largely expanding flux tubes, typically associated with the slow and VSSW, is efficient at the coronal base (boosting the mass flux) but rapidly drops with height providing limited energy per particle. The resulting wind is dense and slow [e.g., *Pinto et al*., 2009]. In this paradigm, the solar cycle variation of proton mass flux results from the changing height of energy deposition at the base of each flux tube.

The VSSW is associated with high helium abundance at solar maximum (Figure 6a), but the helium speeds remain systematically lower than those of protons (Figure 5a). We conclude that while some mechanism is enhancing the abundance, helium is either not efficiently accelerated to high speed in the VSSW or some mechanism is eventually limiting its speed. The very high mass flux inferred in the present study for the slow and the VSSW near solar maximum could enhance Coulomb collisions between protons and helium ions at and well above the transition region [*Lie-Svendsen et al*., 2003] thereby uplifting the heavier helium into the corona. This could point to a more important role of proton drag on the transport and release of helium ions from the coronal base to the upper corona in the VSSW. The effect of Coulomb collisions and gravity alone would forbid helium speed faster than the bulk speed of the dominant species but would allow a higher helium abundance.

Invoking an exclusive role of friction in regulating helium abundance is unlikely to explain the similar speeds of helium ions and protons in the solar wind and VSSW. The acceleration of the slow wind occurs for several tens of solar radii above the solar surface where the plasma is thought to become highly collisionless. It seems therefore unlikely that Coulomb frictions alone would transfer sufficient momentum to helium ions to reach supersonic speeds at these heights and other heating mechanisms must be invoked. The lack of solar cycle variation in the relative proton-helium speed in the slowest winds suggests that if a collisionless heating mechanism is at play to increase the speed of helium above the proton speed during the acceleration phase of the slow wind, then some mechanism is also at play to decrease the speed of helium to that of protons. It is unclear if Coulomb collisions would be sufficiently frequent high up in the corona to fulfill this additional role.

## 7. Conclusions

This paper has revealed a number of interesting features concerning the slowest winds measured to date in the solar wind. The VSSW has a number of interesting properties that suggest it may be the interplanetary signature of long HPS crossings. If this is true, and in light of the analysis of its composition presented here,

a future study should investigate the cycle evolution of the helium abundance of identified HPS crossings measured near 1 AU. We also conclude that the effect of friction in the corona should be revisited and compared with the effect of collisionless processes in regulating helium abundance in the coronal regions associated with very high mass fluxes such as the source regions of the slow and VSSW. The solar cycle variation of the helium abundance could be related to a cycle variation of the rate of Coulomb collisions as solar activity approaches its maximum phase boosting the flux of helium in the corona that becomes available for acceleration in the slow and VSSW. This hypothesis would explain the low abundance of helium during the recent very deep minimum preceding solar cycle 24 [*Kasper et al.*, 2012]. This period coincides with a period of large isolated coronal holes but with very low photospheric magnetic field strength associated with generally lower solar wind mass flux [*McComas et al.*, 2008]. Ongoing modeling work and future observations by Solar Orbiter and Solar Probe will be decisive to further our understanding of the properties and origin of the very slow solar wind. In a future modeling study, we will quantify the role of drag on helium using realistic solar cycle variations in the topological structure of the corona.

**Acknowledgments**

This work has been done in the frame of the HELCATS project (http://www.helcats-fp7.eu), funded by the European Union within the Seventh Framework Programme for Research (FP7 project 606692). We would like to thank the Helios team and NASA's National Space Science Data Center, Space Physics Data Facility, for supplying the plasma and magnetic field data (ftp://spdf.gsfc.nasa.gov/pub/data/helios/), the Mount Wilson Observatory (http://obs.astro.ucla.edu/intro.html), and the Wilcox Solar Observatory for providing the Carrington maps (http://wso.stanford.edu/synopticl.html). We acknowledge Yi-Ming Wang, of the Naval Research Laboratory, for providing the PFSS reconstructions. We acknowledge usage of the tools made available by the French plasma physics data center (Centre de Données de la Physique des Plasmas; CDPP; http://cdpp.eu/), CNES and the space weather team in Toulouse (Solar-Terrestrial Observations and Modelling Service; STORMS). This includes the data mining tools AMDA (http://amda.cdpp.eu/) and the CLWEB tool (clweb.cesr.fr/).

## References

Aellig, M., A. Lazarus, and J. Steinberg (2001), The solar wind helium abundance variation with wind speed and the solar cycle, *Geophys. Res. Lett.*, *28*, 2767–2770, doi:10.1029/2000GL012771.

Barnes, A. (1968), Collisionless heating of the solar-wind plasma: I. Theory of the heating of collisionless plasma by hydromagnetic waves, *Astrophys. J.*, *154*, 751–759.

Bavassano, B., R. Woo, and R. Bruno (1997), Heliospheric plasma sheet and coronal streamers, *Geophys. Res. Lett.*, *24*, 1655–1658, doi:10.1029/97GL01630.

Borrini, G., J. T. Gosling, S. J. Bame, W. C. Feldman, and J. M. Wilcox (1981), Solar wind helium and hydrogen structure near the heliospheric current sheet: A signal of coronal streamers at 1 AU, *J. Geophys. Res.*, *86*(A6), 4565–4573, doi:10.1029/JA086iA06p04565.

Burlaga, L. F. (1995), *Interplanetary Magnetohydrodynamics*, *International Series in Astronomy and Astrophysics*, vol. 3, Oxford Univ. Press, New York.

Collard, H. R., J. D. Mihailov, and J. H. Wolfe (1982), Radial variation of the solar wind speed between 1 and 15 AU, *J. Geophys. Res.*, *87*, 2203–2214, doi:10.1029/JA087iA04p02203.

Crooker, N. U., C.-L. Huang, S. M. Lamassa, D. E. Larson, S. W. Kahler, and H. E. Spence (2004), Heliospheric plasma sheets, *J. Geophys. Res.*, *109*, A03107, doi:10.1029/2003JA010170.

de Toma, G. (2011), Evolution of coronal holes and implications for high-speed solar wind during the minimum between cycles 23 and 24, *Solar Phys.*, *274*, 195–217.

Dusenbery, P. B., and J. V. Hollweg (1981), Ion-cyclotron heating and acceleration of solar wind minor ions, *J. Geophys. Res.*, *86*(A1), 153–164, doi:10.1029/JA086iA01p00153.

Ebert, R. W., D. J. McComas, H. A. Elliott, R. J. Forsyth, and J. T. Gosling (2009), Bulk properties of the slow and fast solar wind and interplanetary coronal mass ejections measured by Ulysses: Three polar orbits of observations, *J. Geophys. Res.*, *114*, A01109, doi:10.1029/2008JA013631.

Feldman, U., E. Landi, and A. Schwadron (2005), On the sources of fast and slow solar wind, *J. Geophys. Res.*, *110*, A07109, doi:10.1029/2004JA010918.

Geiss, J., G. Gloecker, and R. von Steiger (1995), Origine of the solar wind from composition data, *Space Sci. Rev.*, *72*, 49–60.

Geranios, A. (1982), Long period observations of the solar wind plasma between 0.3 AU and 1 AU—Solar activity, *Solar Phys.*, *81*, 333–343.

Gosling, J. T., and V. J. Pizzo (1999), Formation and evolution of corotating interaction regions and their three dimensional structure, *Space Sci. Rev.*, *1*, 21–52, doi:10.1023/A:1005291711900.

Hollweg, J. V., and P. A. Isenberg (2002), Generation of the fast solar wind: A review with emphasis on the resonant cyclotron interaction, *J. Geophys. Res.*, *107*(A7), 1147, doi:10.1029/2001JA000270.

Hundhausen, A. J., S. J. Bame, J. R. Asbridge, and S. J. Sydoriak (1970), Solar wind proton properties: Vela 3 observations from July 1965 to June 1967, *J. Geophys. Res.*, *75*(25), 4643–4657, doi:10.1029/JA075i025p04643.

Kasper, J. C., M. L. Stevens, A. J. Lazarus, J. T. Steinberg, and K. W. Olgivie (2007), Solar wind helium abundance as a function of speed and heliographic latitude: Variation through a solar cycle, *Astrophys. J.*, *660*, 901–910.

Kasper, J. C., A. J. Lazarus, and S. P. Gary (2008), Hot solar-wind helium: Direct evidence for local heating by alfvén-cyclotron dissipation, *Phys. Rev. Lett.*, *101*, 261103, doi:10.1103/PhysRevLett.101.261103.

Kasper, J. C., M. L. Stevens, K. E. Korreck, B. A. Maruca, K. K. Kiefer, N. A. Schwadron, and S. T. Lepri (2012), Evolution of the relationships between helium abundance, minor ion charge state, and solar wind speed over the solar cycle, *Astrophys. J.*, *745*, 162–167.

Lie-Svendsen, Ø., V. H. Hansteen, and E. Leer (2003), Helium abundance in the corona and solar wind: Gyrotropic modeling from the chromosphere to 1 AU, *Astrophys. J.*, *596*, 621–645.

Liu, Y., J. D. Richardson, and J. W. Belcher (2005), A statistical study of the properties of interplanetary coronal mass ejections from 0.3 to 5.4 AU, *Planet. Space Sci.*, *53*, 3–17.

Lopez, R. E., and J. W. Freeman (1986), Solar wind proton temperature-velocity relationship, *J. Geophys. Res.*, *91*(A2), 1701–1705, doi:10.1029/JA091iA02p01701.

Maneva, Y. G., L. Ofman, and A. Viñas (2015), Relative drifts and temperature anisotropies of protons and $\alpha$ particles in the expanding solar wind: 2.5D hybrid simulations, *Astron. Astrophys.*, *579*(A85), 12.

Marsch, E., H. Rosenbauer, R. Schwenn, K. H. Muehlaeuser, and F. M. Neugebauer (1982a), Solar wind helium ions—Observations of the Helios solar probes between 0.3 and 1 AU, *J. Geophys. Res.*, *87*, 35–51, doi:10.1029/JA087iA01p00035.

Marsch, E., R. Schwenn, H. Rosenbauer, K. H. Muehlaeuser, W. Pilipp, and F. M. Neugebauer (1982b), Solar wind protons—Three dimensional distributions and derived plasma parameters measured between 0.3 and 1~AU, *J. Geophys. Res.*, *87*, 52–72, doi:10.1029/JA087iA01p00052.

McComas, D. J., B. L. Barraclough, H. O. Funsten, J. T. Gosling, E. Santiago-Munoz, R. M. Skoug, B. E. Goldstein, M. Neugebauer, P. Riley, and A. Balogh (2000), Solar wind observations over Ulysses' first polar orbit, *J. Geophys. Res.*, *105*, 10,419–10,433, doi:10.1029/1999JA000383.

McComas, D. J., R. W. Ebert, H. A. Elliott, B. E. Goldstein, J. T. Gosling, N. A. Schwadron, and R. M. Skoug (2008), Weaker solar wind from the polar coronal holes and the whole Sun, *Geophys. Res. Lett.*, *35*, L18103, doi:10.1029/2008GL034896.

Ousley, G. W., A. Kutzer, H. J. Panitz (1976), The Helios program and the Sun, paper presented at 27th *International Astronautical Federation Congress, International Astronautical Federation*, Anaheim, Calif.
Pinto, R., R. Grappin, Y.-M. Wang, and J. Leorat (2009), Time-dependent hydrodynamical simulations of slow solar wind, coronal inflows, and polar plumes, *Astron. Astrophys.*, *497*, 537–543.
Pizzo, V. (1978), A three-dimensional model of corotating streams in the solar wind. I—Theoretical foundations, *J. Geophys. Res.*, *83*, 5563–5572, doi:10.1029/JA083iA12p05563.
Pizzo, V. J. (1980), A three-dimensional model of corotating streams in the solar wind. II—Hydrodynamic streams, *J. Geophys. Res.*, *85*, 727–743, doi:10.1029/JA085iA02p00727.
Pizzo, V. J. (1982), A three-dimensional model of corotating streams in the solar wind. III—Magnetohydrodynamic streams, *J. Geophys. Res.*, *87*, 4374–4394, doi:10.1029/JA087iA06p04374.
Rouillard, A. P., et al. (2010a), Intermittent release of transients in the slow solar wind: 1. Remote sensing observations, *J. Geophys. Res.*, *115*, A04103, doi:10.1029/2009JA014471.
Rouillard, A. P., et al. (2010b), Intermittent release of transients in the slow solar wind: 2. In situ evidence, *J. Geophys. Res.*, *115*, A04104, doi:10.1029/2009JA014472.
Rouillard, A. P., et al. (2011), The solar origin of small interplanetary transients, *Astrophys. J.*, *734*(1), 7, doi:10.1088/0004-637X/734/1/7.
Schatten, K. H., J. M. Wilcox, and N. F. Ness (1969), A model of interplanetary and coronal magnetic fields, *Solar Phys.*, *6*, 442–455.
Sheeley, N. R., et al. (1997), Measurements of flow speeds in the corona between 2 and 30 $R_0$, *Astrophys. J.*, *484*(1), 472–478.
Simunac, K., et al. (2012), The heliospheric plasma sheet observed in situ by three spacecraft over four solar rotations, *Sol. Phys.*, *281*, 423–447.
Tao, C., R. Kataoka, H. Fukunishi, Y. Takahasi, and T. Yokoyama (2005), Magnetic field variations in the Jovian magnetotail induced by solar wind dynamic pressure, *J. Geophys. Res.*, *110*, A11208, doi:10.1029/2004JA010959.
Thieme, K. M., E. Marsch, and H. Rosenbauer (1989), Estimates of the alpha particle heating in the solar wind inside 0.3 AU, *J. Geophys. Res.*, *94*, 2673–2676, doi:10.1029/JA094iA03p02673.
Tokumaru, M., M. Kojima, and K. Fujiki (2010), Solar cycle evolution of the solar wind speed distribution from 1985 to 2008, *J. Geophys. Res.*, *115*, A04102, doi:10.1029/2009JA014628.
von Steiger, R., N. A. Schwadron, S. Hefti, L. A. Fisk, J. Geiss, G. Gloeckler, B. Wilken, R. F. Wimmer-Schweingruber, and T. H. Zurbuchen (2000), Composition of quasi-stationary solar wind flows from Ulysses/solar wind ion composition spectrometer, *J. Geophys. Res.*, *105*, 27,217–27,238, doi:10.1029/1999JA000358.
Wang, Y.-M. (1995), Empirical relationship between the magnetic field and the mass and energy flux in the source regions of the solar wind, *Astrophys. J. Lett.*, *449*, L157–L160.
Wang, Y.-M. (2010), On the relative constancy of the solar wind mass flux at 1 AU, *Astrophys. J. Lett.*, *715*, L121–L127.
Wang, Y.-M., E. Robbrecht, and N. R. Sheeley Jr. (2009), On the weakening of the polar magnetic fields during solar cycle 23, *Astrophys. J.*, *707*, 1372–1386.
Widing, K. G., and U. Feldman (2001), On the Rate of abundance modifications versus time in active region plasmas, *Astrophys. J.*, *555*, 426–434.
Wilcox, J. M., and N. F. Ness (1967), Solar source of the interplanetary sector structure, *Solar Phys.*, *1*, 437–445.
Zurbuchen, T. H., S. Hefti, L. A. Fisk, G. Gloeckler, and R. von Steiger (1999), The transition between fast and slow solar wind from composition data, *Space Sci. Rev.*, *87*, 353–356.